Tectonics

Strain localization at the margins of strong lithospheric domains: Insights from analog models

Elisa Calignano[1], Dimitrios Sokoutis[1,2], Ernst Willingshofer[1], Frédéric Gueydan[1,3], and Sierd Cloetingh[1]

[1]Faculty of Geosciences, Department of Earth Sciences, Utrecht University, Utrecht, Netherlands, [2]Department of Geosciences, University of Oslo, Oslo, Norway, [3]Géosciences Montpellier, Université Montpellier, UMR CNRS 5243, Montpellier, France

Abstract The lateral variation of the mechanical properties of continental lithosphere is an important factor controlling the localization of deformation and thus the deformation history and geometry of intraplate mountain belts. A series of three-layer lithospheric-scale analog models, with a strong domain (SD) embedded at various depths, are presented to investigate the development of topography and deformation patterns by having lateral heterogeneities within a weak continental lithosphere. The experiments, performed at a constant velocity and under normal gravity, indicate that the presence or absence of the SD controls whether deformation is localized or distributed at a lithospheric scale. Deformation and topography localize above the edges of the SD, while the SD region itself is characterized by minor amounts of surficial deformation and topography. The depth of the SD (within the ductile crust, ductile mantle lithosphere, or both) controls the pattern of deformation and thus the topography. The presence of a SD in the ductile crust or in the mantle results in limited surficial topographic effects but large variations in the Moho topography. Strong Moho deflection occurs when the SD is in the ductile crust, while the Moho remains almost flat when the SD is in the mantle. When the SD occupies the ductile lithosphere, the SD is tilted. These analog experiments provide insights into intraplate strain localization and could in particular explain the topography around the Tarim Basin, a lithospheric-scale heterogeneity north of the India-Asia collision zone.

1. Introduction

Continental lithosphere exhibits lateral variation in its mechanical strength, as documented by observations and suggested by mechanical models [*Audet and Bürgmann*, 2011; *Burov*, 2011; *Cloetingh et al.*, 2005; *Ranalli*, 1997; *Tesauro et al.*, 2012]. The long geodynamic history of continents resulted in the juxtaposition of crustal and lithospheric fragments that have been subject to different tectonothermal processes over time [*Wilson*, 1966]. These produced changes in composition and thermal structure that influence the rheology and thus the strength of the lithosphere [*Audet and Bürgmann*, 2011]. Continental margins are the locus of polyphase deformation and associated thermal perturbation related to rifting and passive margin formation, as well as subsequent inversion of the margin during collision while, in contrast, continental cores are usually left relatively nondeformed [*Cloetingh et al.*, 2008].

The lateral variation of strength within the lithosphere has been recognized to be an important factor controlling the localization of deformation in intraplate settings [*Clark et al.*, 2005; *Gueydan et al.*, 2014; *Keep*, 2000; *Midtkandal et al.*, 2013; *Munteanu et al.*, 2013; *Sokoutis et al.*, 2005; *Tommasi et al.*, 1995; *Tommasi and Vauchez*, 1997; *Willingshofer et al.*, 2005; *Ziegler et al.*, 1998]. The patterns and rates of continental deformation are determined by both the forces applied to the lithosphere and by its rheology [*Raimondo et al.*, 2014]. First-order large-scale stress fields associated with active plate tectonic processes interact with lateral heterogeneities in the lithosphere and redistribute strain [*Raimondo et al.*, 2014; *Thatcher*, 2003; *Tommasi et al.*, 1995; *Vauchez et al.*, 1998; *Zoback*, 1992]. GPS observations from the Aegean Region, Middle East, Central Asia, Japan, and western U.S. indicate strong strain localization in continental lithosphere [*Calais et al.*, 2006; *Nyst and Thatcher*, 2004; *Reilinger et al.*, 2006; *Thatcher*, 2003, 2009]. In such diffuse plate boundaries, the deformation can be described by the motion of microplates, characterized by low seismicity and topography and devoid of major structures accommodating deformation, bounded by high-strain belts [*Gordon*, 1998; *Stein and Sella*, 2013]. Such kinematic behavior has been attributed to lateral variation in rheology and intraplate stresses [*Stein and Sella*, 2013]. The Tarim Basin in northwestern China is a key area to understand

the interplay between intraplate strain localization and its surface expression. The region is characterized by the presence of a stable area enclosed by two active orogens, the Tian Shan to the north and the Kunlun to the south [*Chang et al.*, 2014; *Yang and Liu*, 2002].

Previous investigations outlined that localization of deformation along lithospheric structures is strongly controlled by the presence of a strong, brittle sub-Moho mantle [*Brun*, 2002; *Buck*, 1991; *Davy and Cobbold*, 1991; *Gueydan and Précigout*, 2014], while strain becomes distributed when the lithospheric mantle shows entirely ductile behavior. In the latter scenario heterogeneous deformation can be attributed to the presence of inherited strong domains embedded in an overall weak lithosphere. However, uncertainties remain regarding the location at depth of such rheologically stronger domains. Increased strength in the lower crust as well as in the upper lithospheric mantle can result from melt extraction processes that leave a dehydrated residue [*Jackson et al.*, 2004; *Karato*, 1986]. In fact, as demonstrated by rock mechanics experiments, silicate rocks deformed under anhydrous condition are significantly stronger than at hydrous conditions [*Bürgmann and Dresen*, 2008; *Kohlstedt et al.*, 1995; *Rybacki and Dresen*, 2000]. In terms of composition, higher viscosities in the lower crust are associated with the presence of more mafic rocks, like diabase or mafic granulite [*Bürgmann and Dresen*, 2008; *Bystricky and Mackwell*, 2001; *Carter and Tsenn*, 1987; *Ranalli and Murphy*, 1987; *Wilks and Carter*, 1990]. For the upper lithospheric mantle, higher viscosities are associated with depletion of Fe relative to Mg components and reduced water content [*Bürgmann and Dresen*, 2008; *Chopra and Paterson*, 1984; *Hirth and Kohlstedt*, 1996].

Numerous modeling studies investigated the localization of deformation in compressional settings in case of lithospheric weak zones flanked by stronger domains [e.g., *Buiter et al.*, 2009; *Cruden et al.*, 2006; *Ellis et al.*, 1998; *Gorczyk and Vogt*, 2013; *Munteanu et al.*, 2013; *Sokoutis and Willingshofer*, 2011; *Willingshofer et al.*, 2005]. Such models have been successfully applied to examples of rift inversion [*Brun and Nalpas*, 1996; *Cerca et al.*, 2004] or compression of weak orogenic wedges at plate boundaries [*Willingshofer et al.*, 2005]. In contrast to these studies, the present paper focuses on the strain redistribution resulting from the presence of a rheological heterogeneity due to strong regions embedded in a weak lithosphere. We use lithospheric-scale analog models where the depth of a high-viscosity domain is systematically varied, in order to identify characteristic deformation patterns and topography related to heterogeneities seated at different depth in the lithosphere. We also discuss implications for the relationship between topography and lithosphere dynamics, focusing on the feasibility to infer the deep lithospheric structure and rheology from surface deformation patterns. In particular, experimental results are compared with the patterns of surface topography and deep lithospheric structure in the Tarim Basin, in central Asia, in order to contribute to the understanding of the parameters that controlled strain localization around this rigid lithospheric block, as a far-field effect of India-Asia continental collision.

2. Experimental Setup

The initial geometric and rheological conditions adopted for the analog experiments represent a region undergoing compression with mechanical heterogeneities within the lithosphere. In particular, we performed four experiments to test the response of a weak three-layer lithosphere to compression in the presence of a rheologically stronger domain.

2.1. Initial Geometry

Figure 1 illustrates the setup and different geometrical configurations for the performed experiments. Strength envelopes are representative for the very initial stage of deformation (see Appendix A for strength profiles). Beside a reference model characterized by laterally uniform lithosphere (Experiment 1), all other experiments consist of three domains with different mechanical properties: a central block containing a mechanically stronger heterogeneity, named "strong domain" (SD), in the ductile part of the lithosphere, is located in between two blocks sharing the same lithospheric stratification as the reference model. The boundaries between rheologically different domains are vertical and strike perpendicular to the convergence direction. The SD (central block) has a width of 6 cm (120 km in nature) in all experiments. The depth of the SD within the model lithosphere has been systematically varied as shown in Figure 1c.

2.2. Rheology

The reference model lithosphere is characterized by a three-layer rheological stratification, where the strength resides mainly in the upper brittle crust. From top to bottom the reference model lithosphere is
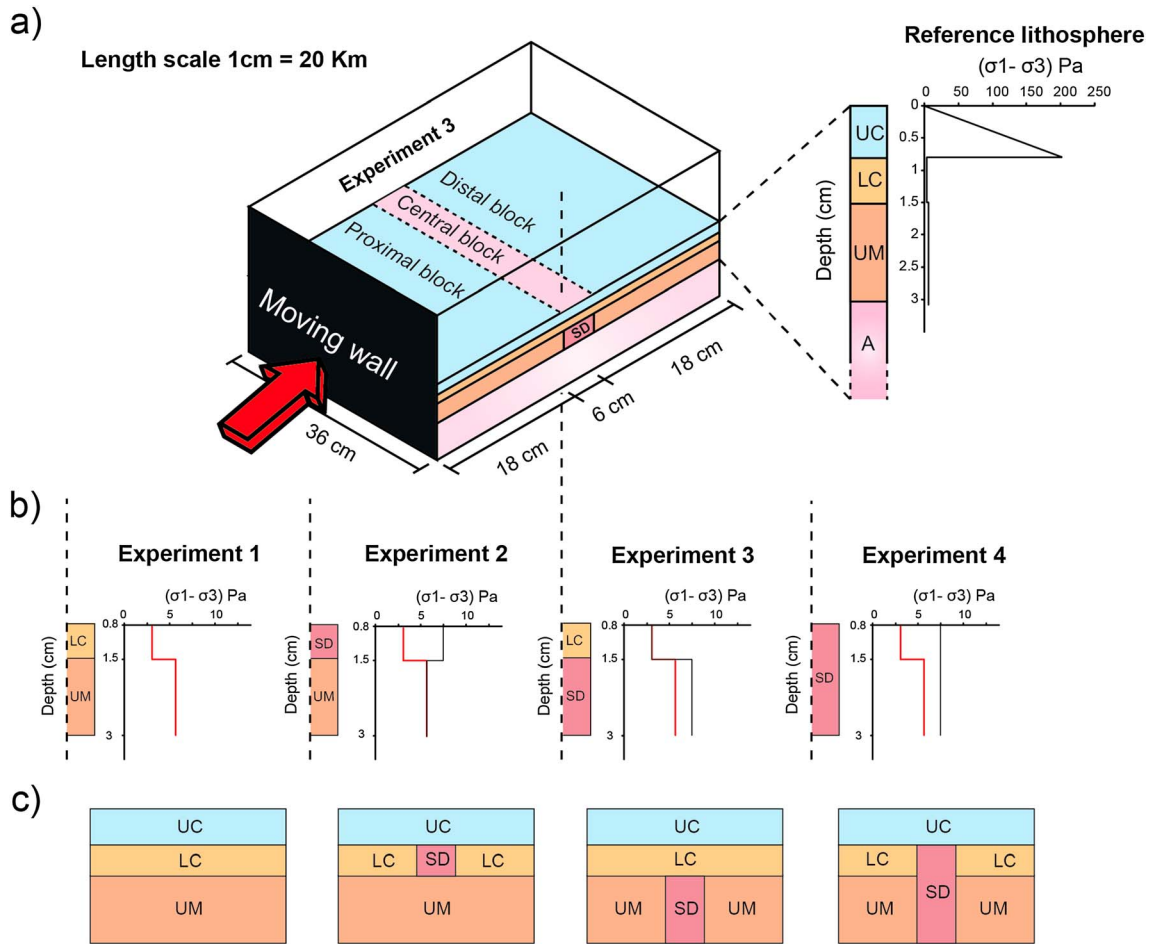
Figure 1. (a) Experimental setup: three-layer laterally heterogeneous continental lithosphere resting on a high-density low-viscosity fluid representing the asthenosphere; shortening is applied via the moving wall; (b) representative strength profiles showing lateral variation in lithospheric strength at initial stage of deformation; red lines represent the strength of the reference lithosphere in experiments 1 to 4, and black lines represent the strong domain; (c) schematic cross section showing the investigated vertical location of the strong domain. UC: upper crust; LC: lower crust; UM: upper mantle; SD: strong domain; and A: asthenosphere.

composed of brittle upper crust, ductile lower crust, and ductile upper mantle (Figure 1). This vertical strength distribution is representative of a weak lithosphere, characteristic of regions with medium-high geothermal gradient [*Afonso and Ranalli*, 2004; *Gueydan et al.*, 2008]. The SD is placed in the ductile regions of the lithosphere (lower crust and upper mantle) for all experiments with a strong heterogeneity.

The brittle upper crust is simulated in our analog experiments with dry feldspar sand. This material is characterized by a linear increase of strength with depth, well representative of a Mohr-Coulomb-type brittle behavior in nature. In the analog models the ductile lower crust and upper lithospheric mantle are

Table 1. Rheological Parameters for the Analog Materials Used in the Experiments

Layer	Material	Density ρ (kg m^{-3})	Coefficient Friction μ	Cohesion C (Pa)	Stress Exponent n[a]	Material Constant A[a]	Effective Viscosity η (Pa s)[a]
Upper crust	Dry feldspar sand	1300	0.4–0.7	15–35			
Lower crust	Silicon 1	1352			1.08	2.00×10^{-5}	4.82×10^{4}
Lithospheric mantle	Silicon 2	1578			1.06	1.00×10^{-5}	9.35×10^{4}
Strong domain	Silicon 3	1555			1.3	6.00×10^{-6}	1.11×10^{5}
Lower lithosphere + asthenosphere	Sodium polytungstate + glycerol	1600					

[a]The values of parameters n, A, and effective viscosity have been determined with a Cony-cylindrical viscometer at a room temperature of 20 ± 2°C.
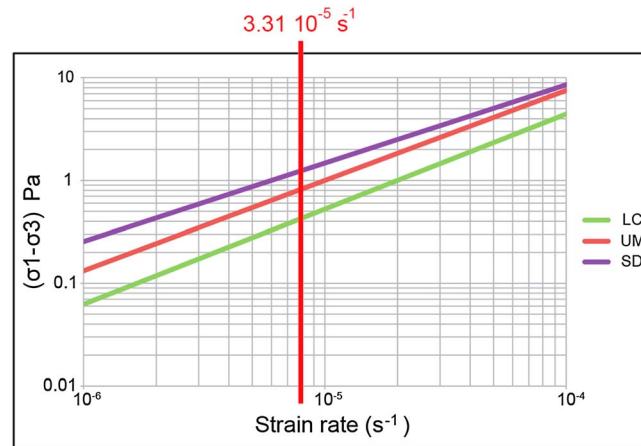
Figure 2. Logarithmic graph of the differential stress versus strain rate for ductile materials used in the experiments. The red vertical line indicates the strain rate corresponding to the applied convergence velocity of 5 cm/h. LC: lower crust; UM: upper mantle; and SD: strong domain.

represented by mixtures of Rhodorsil Gomme (Rhône Poulenc, France) -type silicon, quartz sand, and oleic acid in different proportions to account for differences in density and viscosity between the two layers. The SD is modeled with a mixture of polydimethylsiloxane polymer (PDMS), barium sulphate, and oleic acid, which approximates a stronger ductile behavior than the Rhodorsil Gomme. All three ductile materials deform viscously in a non-Newtonian manner (Table 1). In Figure 2 differential stress-strain rate curves for the experimental ductile materials demonstrate the strength variations between them. For the applied strain rate the silicone mixture used for the SD shows higher ductile resistance than the reference analog lower crust and ductile mantle (Figure 2).

The model lithosphere is resting on a high-density and low-viscosity fluid mixture of polytungstate and glycerol, representing the lower lithospheric mantle and asthenosphere, allowing for isostatic compensation. The density of the ductile lithospheric mantle is lower than the asthenospheric fluid in all experiments, impeding subduction. Mechanical properties of analog materials used in the presented experiments are listed in Table 1.

2.3. Experimental Procedure

The models are built inside a transparent Plexiglas tank with dimensions 36 cm × 50 cm × 15 cm. For the presented experimental series the convergence velocity has been set to 5 cm/h, corresponding to approximately 2 cm/yr in nature. This value can be considered a good mean approximation of continental convergence in nature. Experiments have been performed in a normal gravity field. A total shortening of 8 cm equivalent to 160 km in nature has been applied to all experiments. Boundary effects due to friction along the walls of the box are reduced using glass plates. Deformation is monitored during the experiments with top view pictures and laser scanning at regular time intervals. The conversion of scanner data into digital elevation models (DEMs) allows monitoring of the topographic evolution during convergence. At the end of an experiment the model is cut in cross sections parallel to the convergence direction. This allows the visualization of the internal deformation at the latest experimental stage.

2.4. Scaling

The present series of experiments is not designed to reproduce a specific regional setting but rather to generically investigate the deformation and topography evolution of a lateral heterogeneous continental lithosphere under compression. We, therefore, scaled the experiments to average convergence rates and ductile layers viscosities in nature.

The experiments are scaled according to the criteria of geometrical, rheological, dynamical, and kinematic similarity [*Davy and Cobbold*, 1991; *Ramberg*, 1981; *Weijermars and Schmeling*, 1986]. Scaling parameters for brittle and ductile deformation are presented in Table 2. The length scale factor is 5.0×10^{-7} so that 1 cm in the model corresponds to 20 km in nature.

Dynamic and kinematic similarities have been tested with dimensionless ratios. In particular, for ductile layers the Ramberg number has been calculated as the ratio between gravitational and viscous forces:

$$R_m = \frac{\rho g h_d}{(\sigma_1 - \sigma_3)_{\text{viscous}}} \tag{1}$$

where ρ and h_d are respectively the density and thickness of the ductile layer, g is the acceleration due to gravity ($g = 9.81 \text{ m/s}^2$), and $(\sigma_1 - \sigma_3)_{\text{viscous}}$ is the strength for ductile materials with power law-type behavior

Table 2. Scaling Parameters for Analog Experiments and Natural Prototype

Layer	Density ρ (kg m^{-3})	Thickness h (m)	Effective Viscosity η (Pa s)	Strain Rate (s^{-1})	S_m	R_m
Brittle upper crust model	1,300	0.008			4.28	
Brittle upper crust nature	2,700	16,000			4.93	
Ductile lower crust model	1,352	0.007	4.82×10^4	3.31×10^{-5}		29.12
Ductile lower crust nature	2,900	14,000	1.00×10^{22}	1.0×10^{-15}		19.91
Ductile lithospheric mantle model	1,578	0.015	9.35×10^4	3.31×10^{-5}		40.59
Ductile lithospheric mantle nature	3,300	30,000	2.00×10^{22}	1.0×10^{-15}		24.28

(see Appendix A). Given an experimental velocity of 5 cm/h and assuming a mean lower crustal viscosity in nature of 1.0×10^{22} Pa s, the scaled natural velocity is 1.75 cm/yr.

For brittle deformation, dynamic similarity can be tested with the ratio between gravitational forces and frictional forces which can be considered an analog to the Smoluchowski number defined by *Ramberg* [1981].

$$S_m = \frac{\rho g h}{c + \mu \, \rho g h} \tag{2}$$

where ρ, h, c, and μ are the density, thickness, cohesion, and coefficient of friction of the brittle layer, respectively.

2.5. Simplifications

Ductile behavior in nature is strongly dependent on temperature and consequently varies with depth [*Brace and Kohlstedt*, 1980; *Ranalli*, 1995]. In our experiments the viscosity of the ductile lower crust and mantle is depth invariant, i.e., temperature effect is not taken into account. Previous experiments demonstrated that representing the ductile behavior of the lower crust and lithospheric mantle with uniform viscous material is an acceptable first-order approximation [*Davy and Cobbold*, 1991]. The evolution of topography is presented without taking into account surface processes, like erosion, transport, and deposition of sediments. These processes may lead to stress redistribution and influence the time evolution and localization of deformation [*Burov and Cloetingh*, 1997; *Malavieille*, 2010; *Pinto et al.*, 2010; *Willett et al.*, 1993]. Despite these simplifications, the presented experiments are considered representative of first-order deformation and associated topography in the presence of a laterally heterogeneous weak lithosphere under compression.

3. Experimental Results

The results of the conducted experiments are illustrated with the help of digital elevation models (DEMs) acquired at progressive stages of deformation and pictures of cross sections representative of the final stage. The visualization of brittle structures in cross section is helped by the presence of different color sand layers. The topographic evolution of the system for each experiment is tracked with topographic profiles extracted from the DEMs.

In the description of experiments 2–4 we refer to the "proximal block" as the lithospheric block closest to the moving wall, the "central block" as the one containing the SD, and the "distal block" as the lithospheric domain closest to the fixed back wall (Figure 1). With respect to the convergence direction a "forethrust" is defined by a transport in the direction of the moving wall, whereas a "back thrust" shows opposite vergence.

3.1. Experiment 1-Homogeneous Lithosphere

Experiment 1 (the reference experiment) is characterized by a laterally homogeneous three-layer lithosphere (Figure 1). The ductile crust and mantle have similar rheologies and are weak with respect to the brittle upper crust. Figure 3a shows the evolution of lithospheric deformation and associated topography. After 5% BS (bulk shortening), representing 40 km in nature, a first pop-up structure appears at 21 cm distance from the moving wall. Deformation then propagates simultaneously in both directions outward from the first pop-up where other similar structures develop (pop-ups B and C). With ongoing shortening, pop-down basins are formed and progressively buried between two adjacent pop-ups. Between 10% and 15% BS the first pop-up structure stops being active, while the thrusts bounding the pop-ups B and C continue accumulating
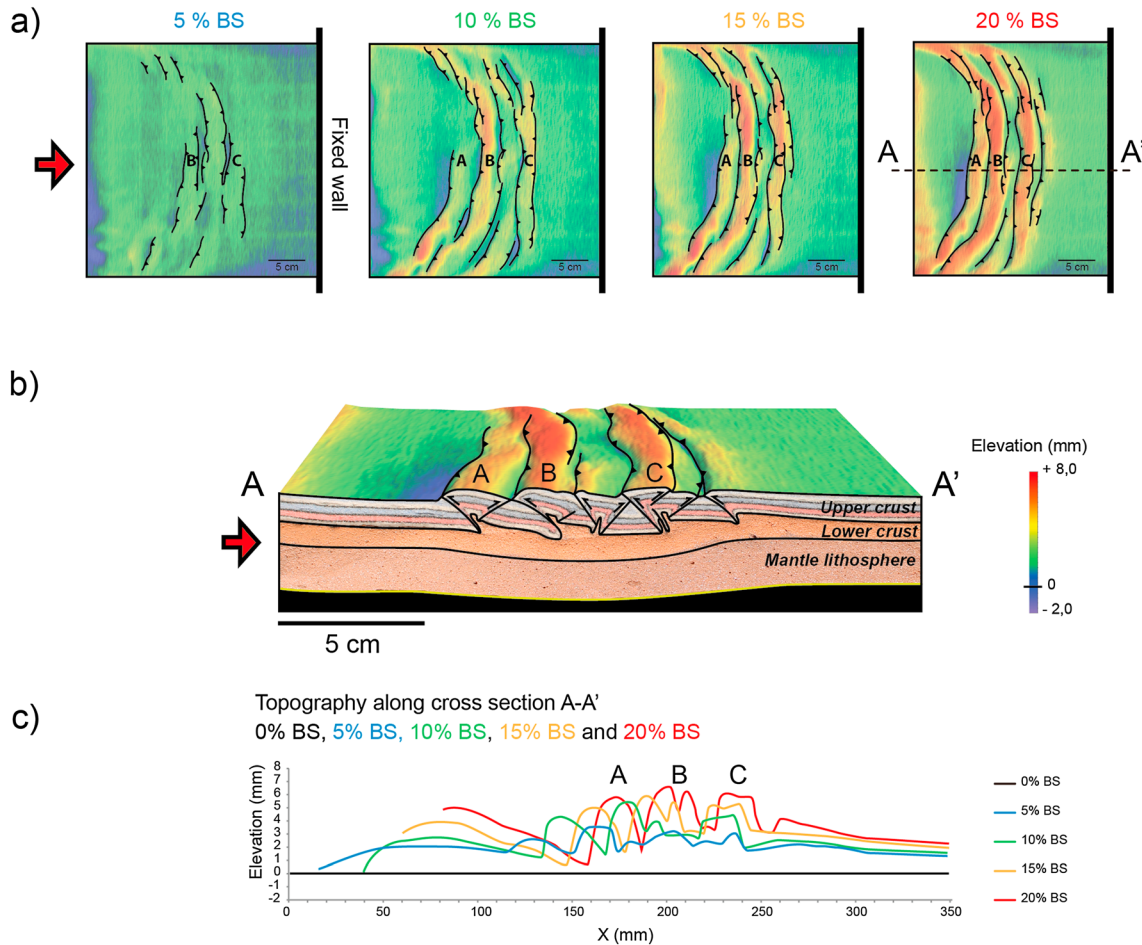
Experiment 1 - homogeneous lithosphere

Figure 3. Modeling results for Experiment 1-homogeneous lithosphere. (a) Evolution of deformation and associated topography shown through DEMs at 5%, 10%, 15%, and 20% bulk shortening. (b) Final geometry and interpreted structures after 20% BS illustrated by a representative cross section (A-A') and DEM. (c) Topography at subsequent deformation stages along the representative section in Figure 3b; labels A, B, and C indicate three main regions of uplift recognized in all models.

shortening and producing uplift. A fourth pop-up structure (pop-up A) appears in the internal part of the active orogen. During the latest stages of shortening a back thrust forms in the model sector facing the fixed back wall. After 20% BS, corresponding to about 160 km of shortening in nature, the deformation is characterized by pop-up and pop-down structures in the brittle crust located in the center of the model. Here the Moho shows a gentle downward deflection and the crust reaches a maximum thickness of about 50 km (Figure 3b). The ductile lower crust is thickened at the location of the Moho deflection, while the thickening of the ductile mantle is more uniformly distributed along the model length (Figure 3b).

3.2. Experiment 2-SD in the Lower Crust

In Experiment 2 the reference lithosphere has been modified by implementing a higher-viscosity SD in the lower crust (Figure 1). The SD is 6 cm wide (equivalent to 120 km in nature) and located in the center of the experimental setup. The strength contrast between the SD and the reference lower crust in the lithosphere of the proximal and distal blocks is illustrated in Figure 2. Figure 4a shows the evolution of lithospheric deformation and surface topography for Experiment 2.

In contrast with the reference experiment, the boundaries of the SD effectively localize deformation from almost the onset of shortening. At 5% BS the main active structure is a back thrust located at the proximal

CALIGNANO ET AL.   401

Experiment 2 - SD in the lower crust
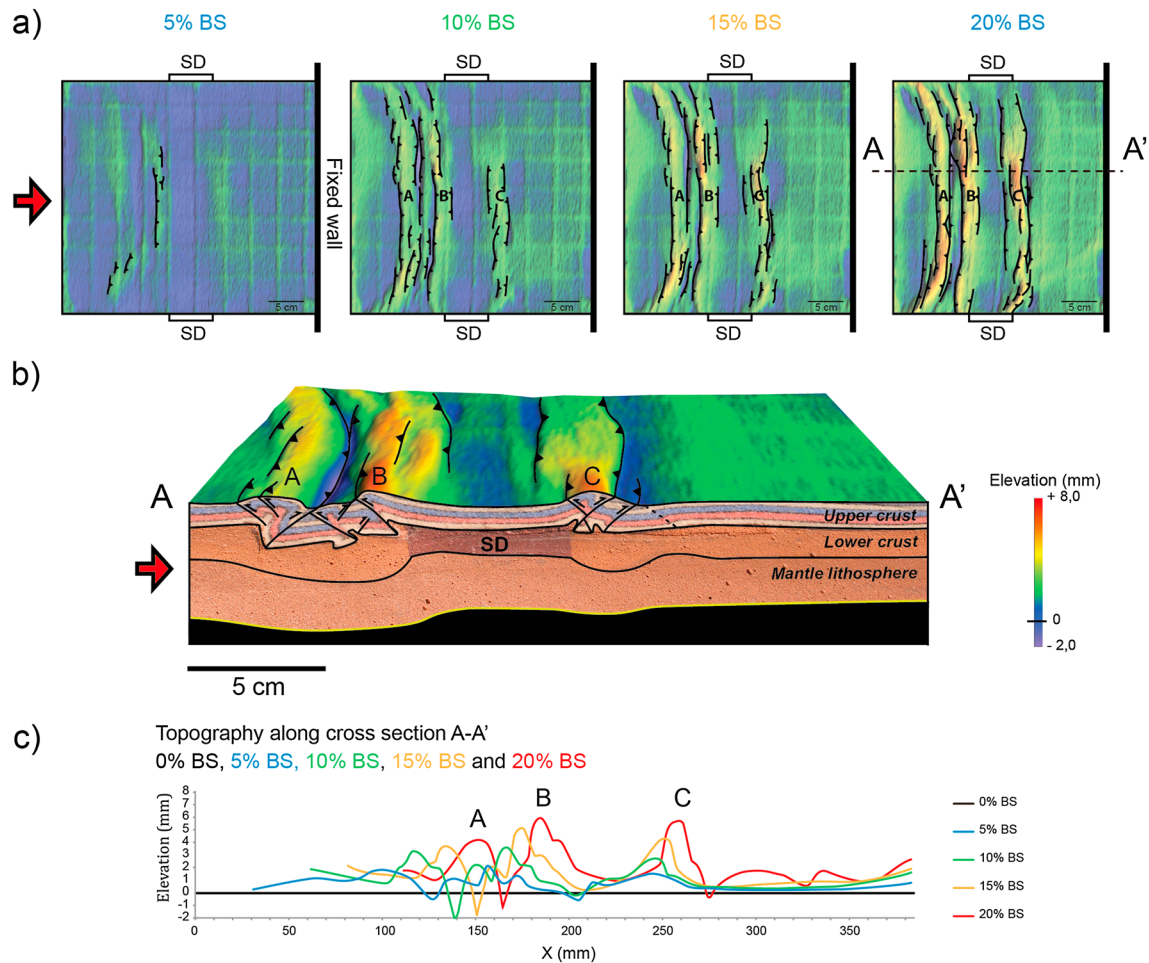
a)

b)

c)

Figure 4. Modeling results for Experiment 2-SD in the lower crust. (a) Evolution of deformation and associated topography shown through DEMs at 5%, 10%, 15%, and 20% bulk shortening. (b) Final geometry and interpreted structures after 20% BS illustrated by a representative cross section (A-A') and DEM. (c) Topography at subsequent deformation stages along the representative section in Figure 4b; labels A, B, and C indicate three main regions of uplift recognized in all models.

boundary of the SD (facing the moving wall). A pop-up structure (pop-up A) in the proximal block of the model forms soon after. With ongoing deformation the thrusts in the proximal block of the model continue to be active while a pop-up structure nucleates at the location of the distal boundary of the SD (pop-up C). After 15% BS a back thrust appears in the distal block. The forward migration of deformation from proximal to distal block is similar to the evolution of Experiment 1. Figure 4b shows the final stage of Experiment 2. Deformation is localized along the boundaries of the lower crustal SD. Two main thrusts with opposite vergence are the main active structures in the brittle upper crust and bound a gentle, downwarped, undeformed region which corresponds to the central block. The Moho and the base of the lithosphere remain at their initial depth (30 km and 60 km, respectively) below the high-viscosity domain, while both horizons are deflected downward underneath the brittle pop-ups and pop-downs. Here the crust reaches a maximum thickness of about 60 km. The SD is virtually undeformed; its length and thickness remain the same as the initial stage.

3.3. Experiment 3-SD in the Lithospheric Mantle

In Experiment 3 the SD has the same width and rheology as in Experiment 2 but is positioned within the ductile lithospheric upper mantle. The lateral contrast in effective viscosity between the SD and reference mantle is indicated in Table 1. The deformation pattern, as observed from surface topography, is similar to Experiment 2, with uplifts occurring along the boundaries of the SD. However, the cross section reveals notable differences in fault patterns and Moho topography (Figure 5b).

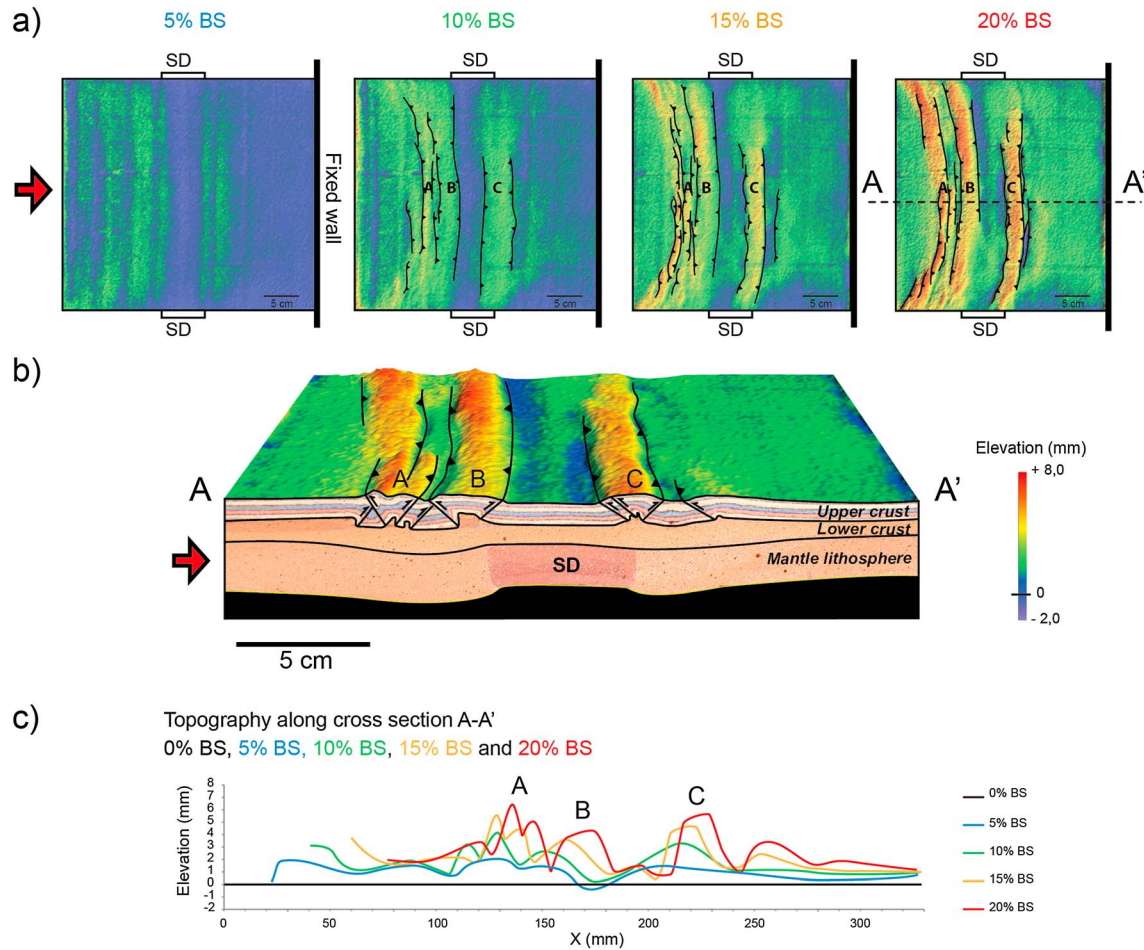## Experiment 3 - SD in the lithospheric mantle

Figure 5. Modeling results for Experiment 3-SD in the lithospheric mantle. (a) Evolution of deformation and associated topography shown through DEMs at 5%, 10%, 15%, and 20% bulk shortening. (b) Final geometry and interpreted structures after 20% BS illustrated by a representative cross section (A-A') and DEM. (c) Topography at subsequent deformation stages along the representative section in Figure 5b; labels A, B, and C indicate three main regions of uplift recognized in all models.

Deformation again localizes at the SD boundaries after 5% BS, as documented by localized uplift (Figure 5a). Subsequently, thrusts with opposite vergence develop at the inflection points of the antiforms, delineating two pop-up structures (pop-ups B and C). With continuing convergence another pop-up appears in the proximal block of the model (pop-up A). A back thrust forms in the distal block at 15% BS. With ongoing convergence, shortening continues to be accommodated along the already formed structures. The pop-ups bounding the central block show a symmetric distribution of shortening between conjugate forethrust and back thrust, quite different from the fault patterns in Experiment 2 (Figure 5b). The Moho is gently deflected upward in the central block and deflected downward at the location of pop-ups and pop-downs in the brittle upper crust where the crust reaches a maximum thickness of 50 km.

3.4. Experiment 4-SD in the Lower Crust and Lithospheric Mantle

In Experiment 4 the SD comprises both the ductile crust and the ductile mantle of the central block (Figure 1). The evolution of deformation at subsequent shortening increments is illustrated in Figure 6a. In contrast to the previous experiments, a strong asymmetry characterizes the deformation pattern and topography due to tilting of the strong lithospheric domain. At 5% BS a forethrust forms in the proximal block of the model. With ongoing convergence a second forethrust develops at the proximal boundary of the SD. By 10% BS
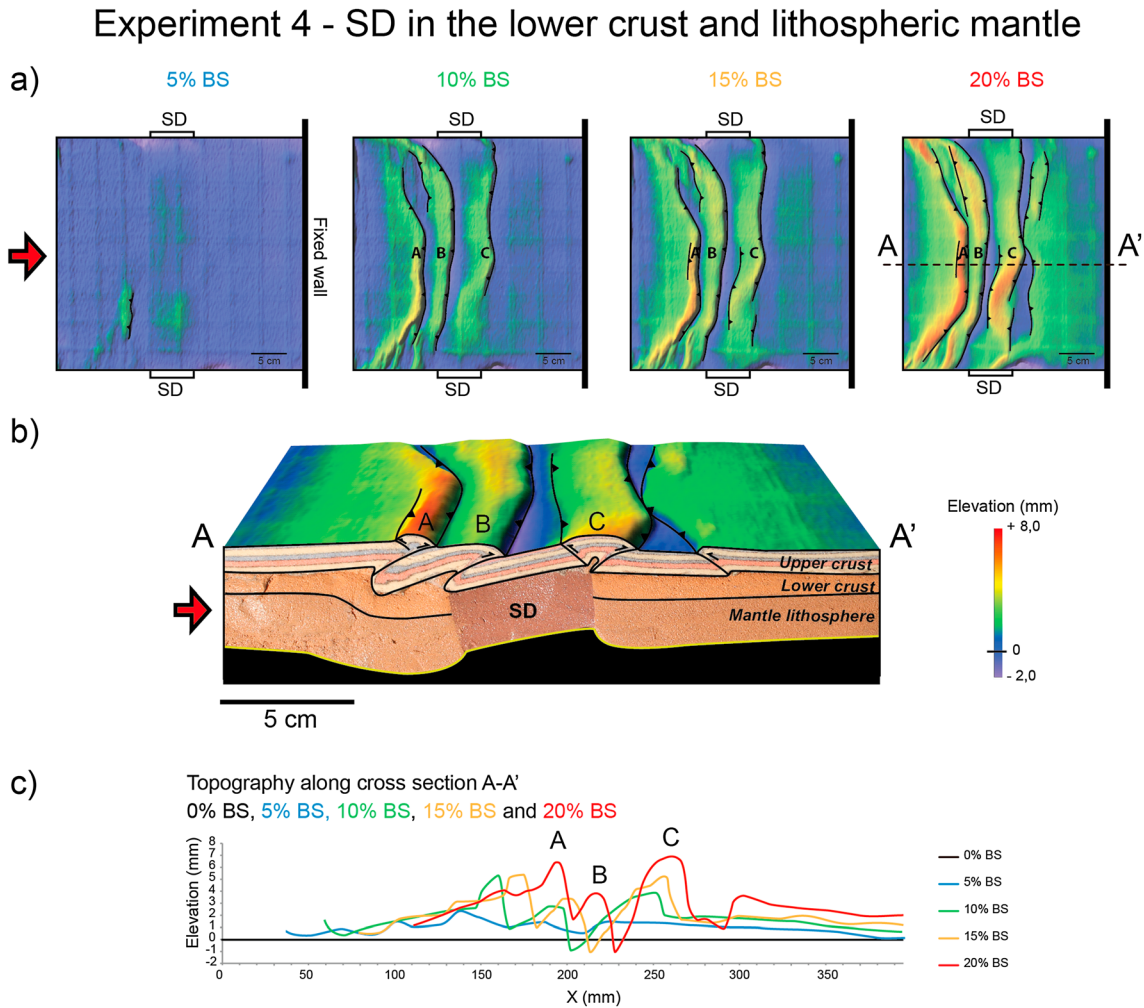
Experiment 4 - SD in the lower crust and lithospheric mantle

Figure 6. Modeling results for Experiments 4-SD in the lower crust and lithospheric mantle. (a) Evolution of deformation and associated topography is shown though DEMs at 5%, 10%, 15%, and 20% bulk shortening. (b) Final geometry and interpreted structures after 20% BS illustrated by a representative cross section (A-A') and DEM. (c) Topography at subsequent deformation stages along the representative section in Figure 6b. Labels A, B, and C indicate three main regions of uplift recognized in all models.

deformation has jumped to the distal boundary of the central block, where an asymmetric pop-up developed (pop-up C). During the latest stages of deformation a back thrust appears in the distal block, bounding a pop-down structure. Shortening in Experiment 4 is accommodated by three main forethrusts, in contrast with previous experiments where deformation was mainly characterized by symmetric pop-ups and -downs. In the cross section of Figure 6b the strong domain is tilted toward the left. The dimension of the SD remains unchanged with respect to the initial configuration, significantly that the SD has undergone insignificant internal deformation. The thickness of the crust reaches its maximum value of approximately 55 km where the first forethrust in the proximal block developed. In the distal lithospheric block the crust is less thickened and reaches a maximum of 45 km (Figure 6b).

3.5. Summary and Interpretation of Experimental Results

Our analog experimental results indicate that effective localization of deformation at vertical rheological boundaries occurs when a high-strength domain is embedded in an overall weak lithosphere.

3.5.1. Common Features

The analysis of the topography and cross sections of the experiments with a SD allows us to identify first-order characteristics independent from its vertical location. Despite the small-strength contrast between the ductile lower crust or mantle and the strong domain (Figure 2), strain becomes localized at the boundaries of the heterogeneity. The behavior of the SD can be considered quasi-rigid since it did not accommodate significant
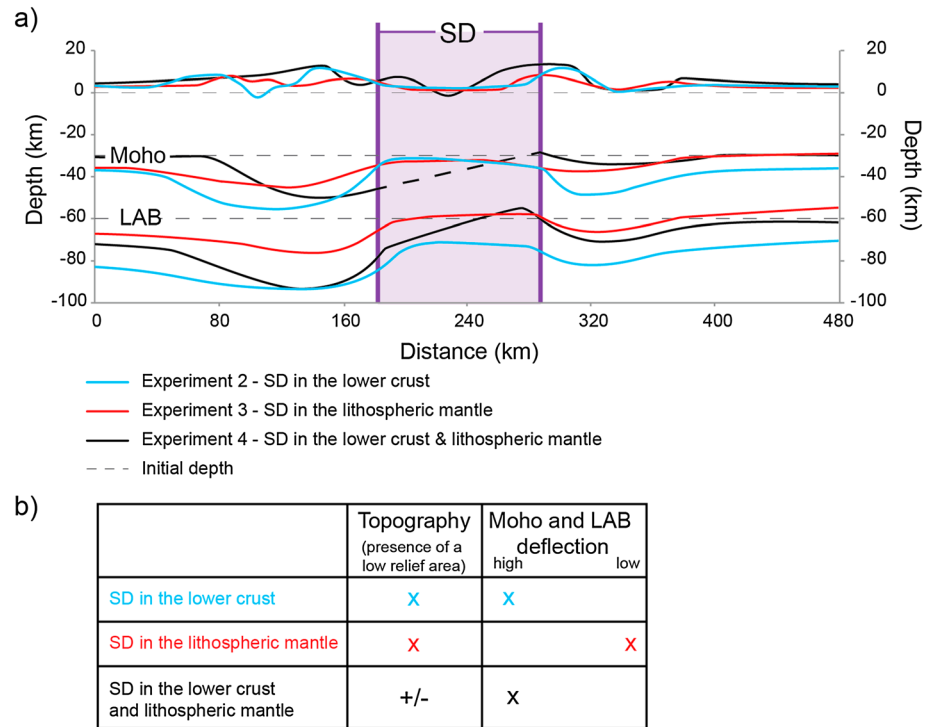
Figure 7. (a) Topography of the surface, Moho, and LAB (lithosphere-asthenosphere boundary) for experiments 2–4 at 20% bulk shortening (BS). (b) Summary of the main characteristics inferred from experiments for surface, Moho, and LAB topographies in relation to the vertical location of the SD.

internal shortening during deformation. Three main elongated uplift belts can be recognized. Of these, the uplift belt closest to the moving wall (region A in Figures 3b, 4b, 5b, and 6b) is most likely a result of asymmetric convergence rather than the presence of a strong heterogeneity in the central block. For the same reason the Moho and lithosphere-asthenosphere boundary (LAB) show a more pronounced downward deflection on the side of the moving wall (Figure 7).

3.5.2. Effect of Depth of the Strong Domain

First-order differences between the experiments concern mainly the geometry of the brittle structures located at the boundaries of the SD (structures B and C in Figures 3b, 4b, 5b, and 6b) and the related Moho and LAB deflection (Figure 7). In particular, the geometries of the Moho and LAB show a strong dependence on the depth of the high-strength domain (Figure 7).

When the lithosphere has a SD within the ductile lower crust, deformation in the brittle upper crust is accommodated by two main thrusts with opposite vergence (Figure 8b). We attribute this result to the inhibition of strain transfer at the strong domain boundaries, causing the observed thickening in the proximal and distal lithospheric block and the pronounced Moho and LAB deflection.

In contrast, when the SD is located in the ductile upper mantle, distributed deformation of the uniform lower crust is responsible for the less pronounced topographic gradients. Two symmetric pop-ups form at the boundaries of the central block, and the Moho and LAB remain at shallower levels (Figure 8c). In both cases, despite the aforementioned differences, an undeformed region characterized by low elevation and topographic gradient becomes enclosed by high-relief narrow belts developing along the boundaries of the SD.

With a SD covering the entire ductile lower crust and upper mantle of the central block, deformation is accommodated by forward thrusts rather than symmetric pop-ups and the low-relief region in the central block is not preserved (Figure 8d). Distributed deformation of the weak ductile lithosphere is in this case inhibited both at the level of the lower crust and ductile mantle by the SD. The SD is tilted toward the moving wall, leading to the development of a central asymmetric basin with higher subsidence on the side of the
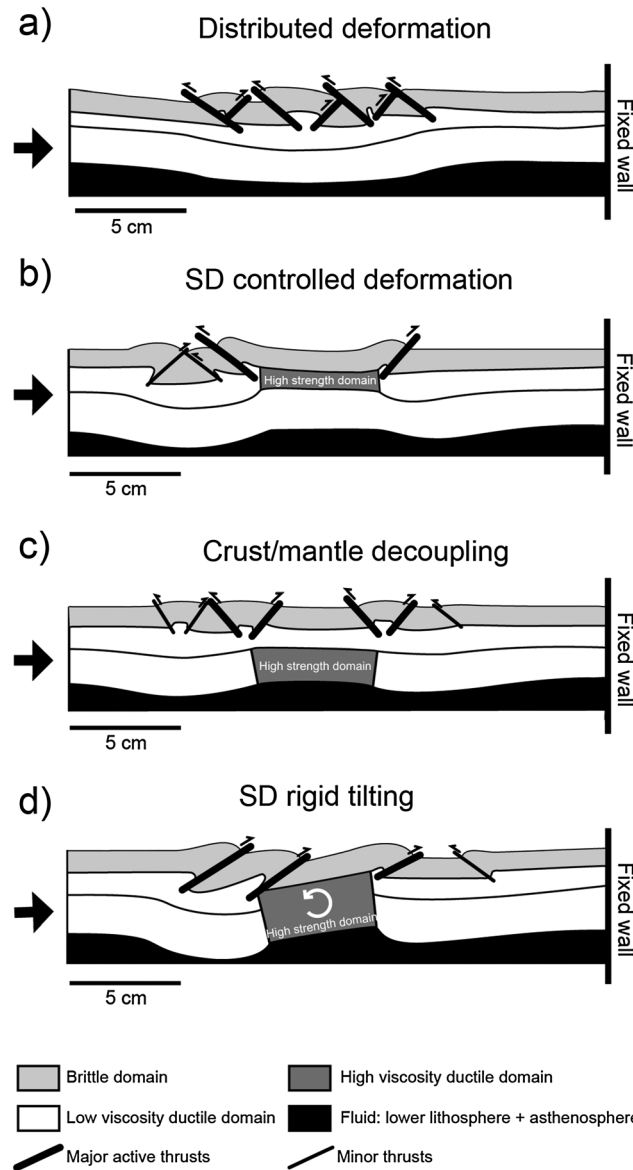
CALIGNANO ET AL.   405

Figure 8. Schematic representation of different fault patterns after 20% BS for (a) a homogeneous lithosphere, (b) a SD located in ductile lower crust, (c) a SD located in the ductile lithospheric mantle, and (d) a SD located in the ductile lower crust and ductile lithospheric mantle.

applied convergence. The Moho and LAB are strongly deflected, reaching higher depths in the proximal block, due to the tilting of the SD (Figure 7).

4. Strain Localization at the Margins of Strong Lithospheric Domains

Compression of a laterally uniform lithosphere, characterized by a purely ductile lithospheric mantle and thus representative of regions with medium-high thermal gradient, results in homogeneous strain distributed over a wide domain (Figure 8a). These results are in agreement with previous experimental studies showing that the absence of a high-strength mantle leads to distributed deformation and thrust systems limited to the upper brittle crust [*Cagnard et al.*, 2006; *Davy and Cobbold*, 1991].

In contrast, deformation strongly localizes when the lithosphere is characterized by lateral rheological heterogeneity. Localization of deformation at the boundaries of rheological heterogeneities has been observed in previous experiments designed to investigate deformation of the lithosphere containing a preexisting weak zone [*Willingshofer et al.*, 2005]. Despite the similarities in the activation of rheological boundaries, the geodynamic evolution of the experiments presented by *Willingshofer et al.* [2005] strongly differs from those observed in our experiments. The nature of the heterogeneity thus governs the evolution of lithospheric deformation and associated topographic development. In the case of a weak lithospheric block flanked by strong lithospheric domains, deformation concentrates inside the weak heterogeneity and high topography develops there [*Sokoutis and Willingshofer*, 2011; *Willingshofer et al.*, 2005]. In the presence of a strong lithospheric domain embedded in a weak lithosphere, deformation focuses outside the boundaries delimiting the strong domain, leaving a topographically low and flat region. In previous geodynamic studies that investigated the localization of deformation in weak zones, the geometry and especially the width of the orogens were strongly dependent on the initial geometry of the weak domain [*Cerca et al.*, 2004; *Ellis et al.*, 1998; *Munteanu et al.*, 2013; *Willingshofer et al.*, 2005]. In our experiments the width of orogenic belts is not a function of the width of the weak lithosphere. In fact, large regions of the surrounding weak lithospheric domains remain undeformed. However, due to the asymmetric convergence imposed in our experiments, the deformed zone in the weak proximal block is wider than the deformed zone in the distal block.

The stability of strong lithospheric domains depends to a large extent on the presence of weaker lithosphere surrounding it [*Lenardic et al.*, 2000; *Yoshida*, 2012]. Our experiments reveal that a viscosity contrast that is smaller than 1 order of magnitude is sufficient to leave the strong lithosphere devoid of deformation.

The importance of rheological heterogeneities for intraplate deformation has been recently proposed by *Munteanu et al.* [2013] for the western Black Sea region. These authors focused their investigation on reactivation of weak domains within the crust, representing a rift event preceding the main compressional phase. In the present study lithospheric-scale models show that the presence of a strong lower crust favors strain localization at the boundaries, thus contributing to intraplate deformation in the weaker domains. Furthermore, we propose that intraplate deformation can also be a response to deeper-seated rheological heterogeneities affecting the lithospheric mantle in combination with a laterally uniform lower crust.

More generally, our experiments illustrate that the presence of a SD causes thickening of the weak lithosphere outside its boundaries and subsequent deepening of both the Moho and the lithosphere-asthenosphere boundary. Recently, a similar geometry characterized by offset of crust and lithosphere thickness at the edges of preexisting lithospheric heterogeneities has been recognized in the Atlas region by *Miller and Becker* [2013]. These authors concluded that such geometric configuration of the lithosphere has been an important factor for the recent channeling of asthenosphere upwelling responsible for the observed magmatism and dynamic topography.

5. Implication for Strain Localization Around the Tarim Basin (Northwestern China)

The Eurasian plate is a well-known example of intraplate deformation associated with the Cenozoic India-Asia continental collision [*Molnar and Tapponnier*, 1975]. Far-field deformation is characterized by uplifting orogenic belts, often bounding rigid and undeformed lithospheric blocks and widespread strike-slip tectonics [*Cunningham*, 2013; *Molnar and Tapponnier*, 1975; *Wang*, 2001]. Prior to the time of India-Asia continental collision, the southern margin of the Eurasian plate has been affected by repeated episodes of terrane accretion and amalgamation linked to the consumption of multiple oceans during Paleozoic and Mesozoic times [*Xiao et al.*, 2013; *Zhang et al.*, 2013b; *Zheng et al.*, 2013]. In particular, the rigid Tarim block was flanked by intensely deformed accretionary orogens, the Tian Shan to the north and the Tibetan Plateau to the south [*Liu et al.*, 2015; *Zhang et al.*, 2013a]. The Tian Shan orogen formed during Paleozoic times as a result of the accretion of island arcs and microcontinents to the Eurasian margin, associated with the subduction of the Paleo-Asian Ocean. In Late Permian to Middle Triassic, the Tian Shan orogen collided with the northern margin of the Tarim along the Turkestan suture [*Xiao et al.*, 2013]. South of the Tarim block a series of roughly east-west trending blocks were accreted to the southern margin of the Eurasian plate during repeated episodes of arc-continent collision from early Paleozoic to Late Mesozoic [*Zhu et al.*, 2013]. Thus, prior to India-Asia continental collision, the lithosphere north and south of the Tarim block was weakened by the presence of multiple suture zones, intensely deformed ophiolitic mélanges, and repeated magmatic activity.
In contrast to the complex structure of the flanking orogens, the Tarim block is composed of a Precambrian basement (pre-Neoproterozoic) and late Neoproterozoic to Paleozoic cover sequence [*Zhang et al.*, 2013a]. Final cratonization of the Tarim basement took place during the assemblage of Columbia supercontinent (Paleoproterozoic). In Early Permian, the emplacement of basaltic magmas associated with the presence of a plume is considered the last tectonothermal event recorded by the Tarim craton [*Zhang et al.*, 2013a]. The pronounced lateral rheological heterogeneity between the rigid Tarim and the composite and highly deformed basement of the Tian Shan and Tibetan Plateau offered a favorable condition for strain localization as a response to stresses generated by the India-Asia collision [*Clark and Royden*, 2000; *Molnar and Tapponnier*, 1981; *Neil and Houseman*, 1997]. As a result, the interior of the Tarim Basin experienced little or no deformation, as indicated by reduced seismicity [*Liu et al.*, 2004; *Zhang Guo-Min et al.*, 2005], low heat flow [*Lei et al.*, 2012; *Liu et al.*, 2004], and absence of major fault structures [*Kao et al.*, 2001; *Lei et al.*, 2012; *Li et al.*, 2006; *Liu et al.*, 2004; *Wang et al.*, 2013], while the Paleozoic Tian Shan and Tibetan blocks underwent renewed orogenesis.

Our lithospheric-scale models successfully explain strain localization in intraplate Eurasia induced by India-Asia collision. The lateral contrast in rheology produced during the pre-Cenozoic tectonic evolution of the southern margin of the Eurasian plate is reproduced by the experiments, with the central block representing the
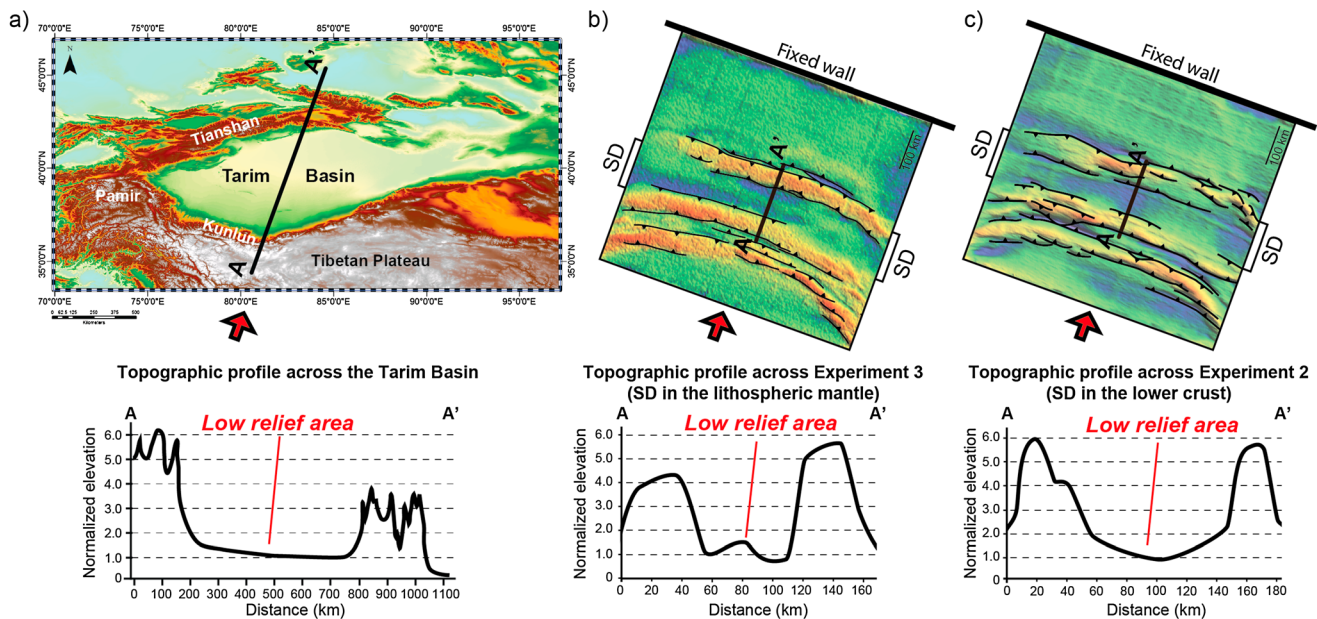
Figure 9. Comparison of experimental results to the Tarim Basin. (a) Relief map of Tarim Basin (northwest China) and topographic profile along a cross section parallel to the India-Asia convergence (N21°E) [*Wang et al.*, 2001]. (b) DEM and topographic profile along a cross section parallel to the convergence direction for Experiment 3. (c) DEM and topographic profile along a cross section parallel to the convergence direction for Experiment 2. Elevation is normalized to the lowest elevation recorded in the low-relief area. The red arrows indicate the direction of convergence.

Tarimblock and the weaker proximal and distal blocks representing the intensely deformed lithosphere of the terrane assemblage north and south the Tarim.

Previous studies interpreted steep topographic gradients flanking such crustal blocks like the Tarim Basin as resulting from oozing of lower crust around rigid obstacles [*Clark and Royden*, 2000]. High-velocity crustal layers, interpreted as mafic, and thus stronger material, emplaced in the middle-lower crust, have been imaged by seismic and tomographic studies, beneath the Tarim Basin and other stable regions in Asia [*Hsü*, 1988; *Li et al.*, 2012; *Wang et al.*, 2013]. These findings, based on analytical models, however, did not investigate the structure beneath the lower crustal flow channel associated with this process. Lithospheric-scale analog models allowed us to expand previous studies including a complex layered lithosphere and to suggest alternative scenarios of strain localization at the margin of stable lithospheric domain that can be applied to the Tarim Basin. In fact, lateral heterogeneities in the lithosphere are not necessarily restricted to crustal levels. Tectonic processes can also modify the rheology and thus the strength of the lithospheric mantle, resulting in lateral heterogeneities at deeper levels [*Gueydan et al.*, 2014; *Vauchez et al.*, 1998; *Ziegler et al.*, 1998]. In the Tarim region, evidences for lateral strength contrasts at mantle depth are provided by tomographic models, showing higher upper mantle seismic velocities with respect to the surrounding regions [*Lei*, 2011].

The comparison between our experiments and the Tarim Basin focuses on the localization of strain at the margins of stable blocks, the associated surface expression, as well as deep lithospheric structure. The plan view architecture of the orogenic belts bounding the Tarim Basin is not considered in this work, due to simplified geometry of the strong domain in our experiments. Figure 9 shows a comparison of a topographic profile across the Tarim Basin and two best fit experiments. The topography of the Tarim Basin (Figure 9a), characterized by a low-relief area enclosed by high-relief belts, is obtained both with a strong domain located in the lower crust and a strong domain located in the lithospheric mantle (Figures 9b and 9c). The highest elevation in experiments 2 and 3 is about 6 times the elevation recorded above the low-relief area corresponding to the strong domain. A similar ratio can be calculated between the highest elevation in the Tibetan Plateau and the elevation of the flat Tarim Basin.

The interpretation of deep seismic profiles suggests a thinner crust within the Tarim Basin (42–45 km) with respect to adjacent regions, where the crust reaches more than 70 km beneath the Tibetan Plateau and 55 km beneath the Tian Shan mountains [*Li et al.*, 2006; *Liu et al.*, 2004]. Areas with high topography correspond to regions of thick crust, whereas low-relief areas correspond to basins and unthickened crust [*Li et al.*, 2012].

The transition between domains of normal crustal thickness to domains of thickened crust is rather sharp: it is characterized by a step in the Moho associated with sudden increase in elevation [*Wang et al.*, 2013]. Such Moho topography is reproduced in our experiments when the SD is located only in the lower crust or lithospheric mantle of the central block (Figure 7). These results, together with the analysis of surface topography, support a scenario where the strength contrast across the Tarim might be located at mantle depths. Heat flow data, seismic activity, and gravity data interpretation suggest for the Tarim block a jelly sandwich type of lithosphere with a strong upper lithospheric mantle [*Liu et al.*, 2004, 2015; *Zhang et al.*, 2013a], implying a higher strength contrast with the surrounding regions than the one investigated in this study. Although our experiments probably underestimate the strength of the Tarim lithospheric mantle, the results consistently suggest that only small-strength contrasts are needed to explain the surface, Moho, and LAB topography of the Tarim and adjacent orogens. We, therefore, argue that a higher integrated strength for the Tarim block would not change the pattern of strain localization but only enhance surface topography, Moho, and LAB gradients at its margins.

Wang et al. [2013] pointed out that in order to postulate the existence of a high-strength domain in the lower crust, that the occurrence of a sharp rise in elevation needs to be accompanied by thickening of the whole crust and associated Moho deepening. This is reflected by a lack of evidence for lateral variation in composition of the lower crust in correspondence to the drop in elevation at the border between the Tibetan Plateau and the stable Sichuan Basin [*Wang et al.*, 2013]. Our experiments support this hypothesis and allow us to introduce a new scenario where a sharp increase in topography and related Moho steps can be the result of the presence of lateral strength contrasts, i.e., a strong domain, located at deeper levels than the lower crust. Lateral heterogeneities in the lithospheric mantle have been imaged beneath the Kyrgyz Tian Shan belt, north of the Tarim, by *Bielinski et al.* [2003] and *Vinnik et al.* [2006]. The interpretation of magnetotelluric profiles across the western Tian Shan leads these authors to recognize a high-resistivity body extending to 100 km depth below the Naryn Basin, a depressed and less deformed area in the central part of the mountain range. The increase in resistivity has been attributed to a decrease in temperature of about 200°C with respect to the adjacent regions or alternatively as a relic of an ocean that was separating the Kazakh block from the Tarim block during Paleozoic [*Bielinski et al.*, 2003]. At the Naryn Basin, the Moho is located at a depth of 35 km while it deepens to 70 km beneath the northern and southern sections of the Tian Shan [*Bielinski et al.*, 2003]. Our experiments illustrate that a strong domain located only in the lithospheric mantle is able to localize deformation at its vertical rheological boundaries. These findings support the hypothesis of previous authors that the high resistivity and therefore strong mantle could have shielded the crust beneath the Naryn Basin from substantial deformation [*Bielinski et al.*, 2003; *Vinnik et al.*, 2006]. A similar mechanism could be responsible for other intermontane basins of the Tian Shan range, including the Issyk Kul and the Chu depression, for which high-velocity bodies at mantle depth have been imaged by *Vinnik et al.* [2006].

6. Conclusions

Analog models were constructed to investigate the behavior of a laterally heterogeneous but overall weak continental lithosphere in compression. The experiments revealed the following:

1. Lateral strength heterogeneities in the lithosphere affect the deformation pattern in compressional settings, perturbing the distributed and homogeneous deformation observed in laterally uniform weak lithosphere subject to compression.
2. Strain localization at the rheological boundaries of a high-viscosity domain, located at different depths of a reference lithosphere, occurs despite small lateral strength variations.
3. The depth of a strong domain in the lithosphere exerts a main control on the location and style of deformation and thus the related topography evolution in time.
4. When the strong domain does not encompass the entire thickness of the ductile region of the lithosphere, deformation can be distributed by ductile thickening at different lithospheric levels.
5. When the rheological heterogeneity comprises the ductile lower crust and upper mantle lithosphere, the strong domain undergoes tilting.
6. Steep topographic gradients may provide important clues for the presence of lateral strength heterogeneities in the lithosphere. Strain localization is manifested in narrow orogenic belts at the boundaries of the strong lithospheric domains, delimiting a stable, low-relief region, as exemplified in the Tarim Basin and surroundings.

Appendix A: Strength Profiles Calculation

The strength profiles presented in Figure 1 represent the very initial deformation stage.

For brittle layers (upper crust) the maximum resistance in compression has been calculated following *Brun* [2002] as

$$(\sigma_1 - \sigma_3)_{\text{brittle}} = 2\,\rho\,g h_b \qquad (A1)$$

where g is the acceleration due to gravity (9.81 m/s^2) and ρ and h_b are the density and thickness of the brittle layer, respectively.

The ductile materials used as analogs for the lower crust and lithospheric mantle deform with a power law-type non-Newtonian behavior (Table 2). Their maximum strength has been calculated according to *Corti et al.* [2004] as

$$(\sigma_1 - \sigma_3)_{\text{viscous}} = 2\left(\frac{\dot{\varepsilon}}{A}\right)^{1/n} \qquad (A2)$$

where $\dot{\varepsilon}$ is the longitudinal strain rate ($\dot{\varepsilon} = \text{velocity}/\text{length}$), A is a material parameter function of pressure, temperature, and material properties, and n is the stress exponent.

References

Afonso, J. C., and G. Ranalli (2004), Crustal and mantle strengths in continental lithosphere: Is the jelly sandwich model obsolete?, *Tectonophysics*, *394*, 221–232, doi:10.1016/j.tecto.2004.08.006.

Audet, P., and R. Bürgmann (2011), Dominant role of tectonic inheritance in supercontinent cycles, *Nat. Geosci.*, *4*, 184–187, doi:10.1038/ngeo1080.

Bielinski, R. A., S. K. Park, A. Rybin, V. Batalev, S. Jun, and C. Sears (2003), Lithospheric heterogeneity in the Kyrgyz Tien Shan imaged by magnetotelluric studies, *Geophys. Res. Lett.*, *30*(15), 1806, doi:10.1029/2003GL017455.

Brace, W. F., and D. L. Kohlstedt (1980), Limits on lithospheric stress imposed by laboratory experiments, *J. Geophys. Res.*, *85*, 6248–6252, doi:10.1029/JB085iB11p06248.

Brun, J.-P. (2002), Deformation of the continental lithosphere: Insights from brittle-ductile models, *Geol. Soc. London Spec. Publ.*, *200*, 355–370, doi:10.1144/GSL.SP.2001.200.01.20.

Brun, J.-P., and T. Nalpas (1996), Graben inversion in nature and experiments, *Tectonics*, *15*, 677–687, doi:10.1029/95TC03853.

Buck, W. R. (1991), Modes of continental lithospheric extension, *J. Geophys. Res.*, *96*, 20,161–20,178, doi:10.1029/91JB01485.

Buiter, S. J. H., O. A. Pfiffner, and C. Beaumont (2009), Inversion of extensional sedimentary basins: A numerical evaluation of the localisation of shortening, *Earth Planet. Sci. Lett.*, *288*, 492–504, doi:10.1016/j.epsl.2009.10.011.

Bürgmann, R., and G. Dresen (2008), Rheology of the lower crust and upper mantle: Evidence from rock mechanics, geodesy, and field observations, *Annu. Rev. Earth Planet. Sci.*, *36*, 531–567, doi:10.1146/annurev.earth.36.031207.124326.

Burov, E., and S. Cloetingh (1997), Erosion and rift dynamics: New thermomechanical aspects of post-rift evolution of extensional basins, *Earth Planet. Sci. Lett.*, *150*, 7–26, doi:10.1016/S0012-821X(97)00069-1.

Burov, E. B. (2011), Rheology and strength of the lithosphere, *Mar. Petrol. Geol.*, *28*, 1402–1443, doi:10.1016/j.marpetgeo.2011.05.008.

Bystricky, M., and S. Mackwell (2001), Creep of dry clinopyroxene aggregates, *J. Geophys. Res.*, *106*, 13,443–13,454, doi:10.1029/2001JB000333.

Cagnard, F., J.-P. Brun, and D. Gapais (2006), Modes of thickening of analogue weak lithospheres, *Tectonophysics*, *421*, 145–160, doi:10.1016/j.tecto.2006.04.016.

Calais, E., L. Dong, M. Wang, Z. Shen, and M. Vergnolle (2006), Continental deformation in Asia from a combined GPS solution, *Geophys. Res. Lett.*, *33*, L24319, doi:10.1029/2006GL028433.

Carter, N. L., and M. C. Tsenn (1987), Flow properties of continental lithosphere, *Tectonophysics*, *136*, 27–63, doi:10.1016/0040-1951(87)90333-7.

Cerca, M., L. Ferrari, M. Bonini, G. Corti, and P. Manetti (2004), The role of crustal heterogeneity in controlling vertical coupling during Laramide shortening and the development of the Caribbean-North America transform boundary in southern Mexico: Insights from analogue models, *Geol. Soc. London Spec. Publ.*, *227*, 117–139, doi:10.1144/GSL.SP.2004.227.01.07.

Chang, H., Z. An, W. Liu, H. Ao, X. Qiang, Y. Song, and Z. Lai (2014), Quaternary structural partitioning within the rigid Tarim plate inferred from magnetostratigraphy and sedimentation rate in the eastern Tarim Basin in China, *Quatern. Res.*, *81*, 424–432, doi:10.1016/j.yqres.2013.10.018.

Chopra, P. N., and M. S. Paterson (1984), The role of water in the deformation of dunite, *J. Geophys. Res.*, *89*, 7861–7876, doi:10.1029/JB089iB09p07861.

Clark, M. K., and L. H. Royden (2000), Topographic ooze: Building the eastern margin of Tibet by lower crustal flow, *Geology*, *28*, 703–706, doi:10.1130/0091-7613(2000)28<703:TOBTEM>2.0.CO;2.

Clark, M. K., J. W. M. Bush, and L. H. Royden (2005), Dynamic topography produced by lower crustal flow against rheological strength heterogeneities bordering the Tibetan Plateau, *Geophys. J. Int.*, *162*, 575–590, doi:10.1111/j.1365-246X.2005.02580.x.

Cloetingh, S., P. A. Ziegler, F. Beekman, P. A. M. Andriessen, L. Matenco, G. Bada, D. Garcia-Castellanos, N. Hardebol, P. Dèzes, and D. Sokoutis (2005), Lithospheric memory, state of stress and rheology: Neotectonic controls on Europe's intraplate continental topography, *Quat. Sci. Rev.*, *24*, 241–304, doi:10.1016/j.quascirev.2004.06.015.

Cloetingh, S., F. Beekman, P. A. Ziegler, J.-D. van Wees, and D. Sokoutis (2008), Post-rift compressional reactivation potential of passive margins and extensional basins, *Geol. Soc. London Spec. Publ.*, *306*, 27–70, doi:10.1144/SP306.2.

Corti, G., M. Bonini, D. Sokoutis, F. Innocenti, P. Manetti, S. Cloetingh, and G. Mulugeta (2004), Continental rift architecture and patterns of magma migration: A dynamic analysis based on centrifuge models, *Tectonics*, *23*, TC2012, doi:10.1029/2003TC001561.

Cruden, A. R., M. H. B. Nasseri, and R. Pysklywec (2006), Surface topography and internal strain variation in wide hot orogens from three-dimensional analogue and two-dimensional numerical vice models, *Geol. Soc. Lond. Spec. Publ.*, *253*, 79–104, doi:10.1144/GSL.SP.2006.253.01.04.

Cunningham, D. (2013), Mountain building processes in intracontinental oblique deformation belts: Lessons from the Gobi Corridor, Central Asia, *J. Struct. Geol.*, *46*, 255–282, doi:10.1016/j.jsg.2012.08.010.

Davy, P., and P. R. Cobbold (1991), Experiments on shortening of a 4-layer model of the continental lithosphere, *Tectonophysics*, *188*, 1–25, doi:10.1016/0040-1951(91)90311-F.

Ellis, S., C. Beaumont, R. A. Jamieson, and G. Quinlan (1998), Continental collision including a weak zone: The vise model and its application to the Newfoundland Appalachians, *Can. J. Earth Sci.*, *35*, 1323–1346, doi:10.1139/e97-100.

Gorczyk, W., and K. Vogt (2013), Tectonics and melting in intra-continental settings, *Gondwana Res.*, doi:10.1016/j.gr.2013.09.021.

Gordon, R. G. (1998), The plate tectonic approximation: Plate nonrigidity, diffuse plate boundaries, and global plate reconstructions, *Annu. Rev. Earth Planet. Sci.*, *26*, 615–642, doi:10.1146/annurev.earth.26.1.615.

Gueydan, F., and J. Précigout (2014), Modes of continental rifting as a function of ductile strain localization in the lithospheric mantle, *Tectonophysics*, *612–613*, 18–25, doi:10.1016/j.tecto.2013.11.029.

Gueydan, F., C. Morency, and J.-P. Brun (2008), Continental rifting as a function of lithosphere mantle strength, *Tectonophysics*, *460*, 83–93, doi:10.1016/j.tecto.2008.08.012.

Gueydan, F., J. Précigout, and L. G. J. Montési (2014), Strain weakening enables continental plate tectonics, *Tectonophysics*, *631*, 189–196, doi:10.1016/j.tecto.2014.02.005.

Hirth, G., and D. L. Kohlstedt (1996), Water in the oceanic upper mantle: Implications for rheology, melt extraction and the evolution of the lithosphere, *Earth Planet. Sci. Lett.*, *144*, 93–108, doi:10.1016/0012-821X(96)00154-9.

Hsü, K. J. (1988), Relict back-arc basins: Principles of recognition and possible new examples from China, in *New Perspectives in Basin Analysis*, edited by K. L. Kleinspehn and C. Paola, pp. 245–263, Springer, New York.

Jackson, J. A., H. Austrheim, D. McKenzie, and K. Priestley (2004), Metastability, mechanical strength, and the support of mountain belts, *Geology*, *32*, 625–628, doi:10.1130/g20397.1.

Kao, H., R. Gao, R.-J. Rau, D. Shi, R.-Y. Chen, Y. Guan, and F. T. Wu (2001), Seismic image of the Tarim basin and its collision with Tibet, *Geology*, *29*, 575–578, doi:10.1130/0091-7613(2001)029<0575:siottb>2.0.co;2.

Karato, S. (1986), Does partial melting reduce the creep strength of the upper mantle?, *Nature*, *319*, 309–310.

Keep, M. (2000), Models of lithospheric-scale deformation during plate collision: Effects of indentor shape and lithospheric thickness, *Tectonophysics*, *326*, 203–216, doi:10.1016/S0040-1951(00)00123-2.

Kohlstedt, D. L., B. Evans, and S. J. Mackwell (1995), Strength of the lithosphere: Constraints imposed by laboratory experiments, *J. Geophys. Res.*, *100*, 17,587–17,602, doi:10.1029/95JB01460.

Lei, J. (2011), Seismic tomographic imaging of the crust and upper mantle under the central and western Tien Shan orogenic belt, *J. Geophys. Res.*, *116*, B09305, doi:10.1029/2010JB008000.

Lei, R., C. Wu, G. Chi, G. Chen, L. Gu, and Y. Jiang (2012), Petrogenesis of the Palaeoproterozoic Xishankou pluton, northern Tarim block, northwest China: Implications for assembly of the supercontinent Columbia, *Int. Geol. Rev.*, *54*, 1829–1842, doi:10.1080/00206814.2012.678045.

Lenardic, A., L. Moresi, and H. Mühlhaus (2000), The role of mobile belts for the longevity of deep cratonic lithosphere: The crumple zone model, *Geophys. Res. Lett.*, *27*, 1235–1238, doi:10.1029/1999GL008410.

Li, H., S. Li, X. D. Song, M. Gong, X. Li, and J. Jia (2012), Crustal and uppermost mantle velocity structure beneath northwestern China from seismic ambient noise tomography, *Geophys. J. Int.*, *188*, 131–143, doi:10.1111/j.1365-246X.2011.05205.x.

Li, S., W. D. Mooney, and J. Fan (2006), Crustal structure of mainland China from deep seismic sounding data, *Tectonophysics*, *420*, 239–252, doi:10.1016/j.tecto.2006.01.026.

Liu, S., L. Wang, C. Li, H. Li, Y. Han, C. Jia, and G. Wei (2004), Thermal-rheological structure of lithosphere beneath the northern flank of Tarim Basin, western China: Implications for geodynamics, *Sci. China Ser. D Earth Sci.*, *47*, 659–672, doi:10.1360/03yd0471.

Liu, S., X. Lei, and L. Wang (2015), New heat flow determination in northern Tarim Craton, northwest China, *Geophys. J. Int.*, *200*, 1196–1206, doi:10.1093/gji/ggu458.

Malavieille, J. (2010), Impact of erosion, sedimentation, and structural heritage on the structure and kinematics of orogenic wedges: Analog models and case studies, *GSA Today*, 4–10, doi:10.1130/GSATG48A.1.

Midtkandal, I., J.-P. Brun, R. H. Gabrielsen, and R. S. Huismans (2013), Control of lithosphere rheology on subduction polarity at initiation: Insights from 3D analogue modelling, *Earth Planet. Sci. Lett.*, *361*, 219–228, doi:10.1016/j.epsl.2012.10.026.

Miller, M. S., and T. W. Becker (2013), Reactivated lithospheric-scale discontinuities localize dynamic uplift of the Moroccan Atlas Mountains, *Geology*, doi:10.1130/G34959.1.

Molnar, P., and P. Tapponnier (1975), Cenozoic tectonics of Asia: Effects of a continental collision—Features of recent continental tectonics in Asia can be interpreted as results of the India-Eurasia collision, *Science*, *189*, 419–426, doi:10.1126/science.189.4201.419.

Molnar, P., and P. Tapponnier (1981), A possible dependence of tectonic strength on the age of the crust in Asia, *Earth Planet. Sci. Lett.*, *52*, 107–114, doi:10.1016/0012-821X(81)90213-2.

Munteanu, I., E. Willingshofer, D. Sokoutis, L. Matenco, C. Dinu, and S. Cloetingh (2013), Transfer of deformation in back-arc basins with a laterally variable rheology: Constraints from analogue modelling of the Balkanides-Western Black Sea inversion, *Tectonophysics*, *602*, 223–236, doi:10.1016/j.tecto.2013.03.009.

Neil, E. A., and G. A. Houseman (1997), Geodynamics of the Tarim Basin and the Tian Shan in central Asia, *Tectonics*, *16*, 571–584, doi:10.1029/97TC01413.

Nyst, M., and W. Thatcher (2004), New constraints on the active tectonic deformation of the Aegean, *J. Geophys. Res.*, *109*, B11406, doi:10.1029/2003JB002830.

Pinto, L., C. Muñoz, T. Nalpas, and R. Charrier (2010), Role of sedimentation during basin inversion in analogue modelling, *J. Struct. Geol.*, *32*, 554–565, doi:10.1016/j.jsg.2010.03.001.

Raimondo, T., M. Hand, and W. J. Collins (2014), Compressional intracontinental orogens: Ancient and modern perspectives, *Earth Sci. Rev.*, *130*, 128–153, doi:10.1016/j.earscirev.2013.11.009.

Ramberg, H. (1981), *Gravity, Deformation and the Earth's Crust*, 2nd ed., 452 pp., Academic Press, London.

Ranalli, G. (1995), *Rheology of the Earth*, Springer, New York.

Ranalli, G. (1997), Rheology of the lithosphere in space and time, *Geol. Soc. London Spec. Publ.*, *121*, 19–37, doi:10.1144/GSL.SP.1997.121.01.02.

Ranalli, G., and D. C. Murphy (1987), Rheological stratification of the lithosphere, *Tectonophysics*, *132*, 281–295, doi:10.1016/0040-1951(87)90348-9.

Reilinger, R., et al. (2006), GPS constraints on continental deformation in the Africa-Arabia-Eurasia continental collision zone and implications for the dynamics of plate interactions, *J. Geophys. Res.*, *111*, B05411, doi:10.1029/2005JB004051.

Rybacki, E., and G. Dresen (2000), Dislocation and diffusion creep of synthetic anorthite aggregates, *J. Geophys. Res.*, *105*, 26,017–26,036, doi:10.1029/2000JB900223.

Sokoutis, D., and E. Willingshofer (2011), Decoupling during continental collision and intra-plate deformation, *Earth Planet. Sci. Lett.*, *305*, 435–444, doi:10.1016/j.epsl.2011.03.028.

Sokoutis, D., J.-P. Burg, M. Bonini, G. Corti, and S. Cloetingh (2005), Lithospheric-scale structures from the perspective of analogue continental collision, *Tectonophysics*, *406*, 1–15, doi:10.1016/j.tecto.2005.05.025.

Stein, S., and G. F. Sella (2013), Plate boundary zones: Concepts and approaches, in *Plate Boundary Zones*, edited by S. Stein and J. T. Freymueller, pp. 1–26, AGU, Washington, D. C.

Tesauro, M., P. Audet, M. K. Kaban, R. Bürgmann, and S. Cloetingh (2012), The effective elastic thickness of the continental lithosphere: Comparison between rheological and inverse approaches, *Geochem. Geophys. Geosyst.*, *13*, Q09001, doi:10.1029/2012GC004162.

Thatcher, W. (2003), GPS constraints on the kinematics of continental deformation, *Int. Geol. Rev.*, *45*, 191–212, doi:10.2747/0020-6814.45.3.191.

Thatcher, W. (2009), How the continents deform: The evidence from tectonic geodesy, *Annu. Rev. Earth Planet. Sci.*, *37*, 237–262, doi:10.1146/annurev.earth.031208.100035.

Tommasi, A., and A. Vauchez (1997), Continental-scale rheological heterogeneities and complex intraplate tectono-metamorphic patterns: Insights from a case-study and numerical models, *Tectonophysics*, *279*, 327–350, doi:10.1016/S0040-1951(97)00117-0.

Tommasi, A., A. Vauchez, and B. Daudré (1995), Initiation and propagation of shear zones in a heterogeneous continental lithosphere, *J. Geophys. Res.*, *100*, 22,083–22,101, doi:10.1029/95JB02042.

Vauchez, A., A. Tommasi, and G. Barruol (1998), Rheological heterogeneity, mechanical anisotropy and deformation of the continental lithosphere, *Tectonophysics*, *296*, 61–86, doi:10.1016/S0040-1951(98)00137-1.

Vinnik, L. P., I. M. Aleshin, M. K. Kaban, S. G. Kiselev, G. L. Kosarev, S. I. Oreshin, and C. Reigber (2006), Crust and mantle of the Tien Shan from data of the receiver function tomography, *Izv. Phys. Solid Earth*, *42*, 639–651, doi:10.1134/S1069351306080027.

Wang, Q., et al. (2001), Present-day crustal deformation in China constrained by Global Positioning System measurements, *Science*, *294*, 574–577, doi:10.1126/science.1063647.

Wang, Y. (2001), Heat flow pattern and lateral variations of lithosphere strength in China mainland: Constraints on active deformation, *Phys. Earth Planet. In.*, *126*, 121–146, doi:10.1016/S0031-9201(01)00251-5.

Wang, Y., W. D. Mooney, X. Yuan, and N. Okaya (2013), Crustal structure of the northeastern Tibetan Plateau from the Southern Tarim Basin to the Sichuan Basin, China, *Tectonophysics*, *584*, 191–208, doi:10.1016/j.tecto.2012.09.003.

Weijermars, R., and H. Schmeling (1986), Scaling of Newtonian and non-Newtonian fluid dynamics without inertia for quantitative modelling of rock flow due to gravity (including the concept of rheological similarity), *Phys. Earth Planet. In.*, *43*, 316–330, doi:10.1016/0031-9201(86)90021-X.

Wilks, K. R., and N. L. Carter (1990), Rheology of some continental lower crustal rocks, *Tectonophysics*, *182*, 57–77, doi:10.1016/0040-1951(90)90342-6.

Willett, S., C. Beaumont, and P. Fullsack (1993), Mechanical model for the tectonics of doubly vergent compressional orogens, *Geology*, *21*, 371–374, doi:10.1130/0091-7613(1993)021<0371:MMFTTO>2.3.CO;2.

Willingshofer, E., D. Sokoutis, and J.-P. Burg (2005), Lithospheric-scale analogue modelling of collision zones with a pre-existing weak zone, *Geol. Soc. London Spec. Publ.*, *243*, 277–294, doi:10.1144/GSL.SP.2005.243.01.18.

Wilson, J. T. (1966), Did the Atlantic close and then re-open?, *Nature*, *211*, 676–681.

Xiao, W., B. F. Windley, M. B. Allen, and C. Han (2013), Paleozoic multiple accretionary and collisional tectonics of the Chinese Tianshan orogenic collage, *Gondwana Res.*, *23*, 1316–1341, doi:10.1016/j.gr.2012.01.012.

Yang, Y., and M. Liu (2002), Cenozoic deformation of the Tarim plate and the implications for mountain building in the Tibetan Plateau and the Tian Shan, *Tectonics*, *21*(6), 1059, doi:10.1029/2001TC001300.

Yoshida, M. (2012), Dynamic role of the rheological contrast between cratonic and oceanic lithospheres in the longevity of cratonic lithosphere: A three-dimensional numerical study, *Tectonophysics*, *532–535*, 156–166, doi:10.1016/j.tecto.2012.01.029.

Zhang, C.-L., H.-B. Zou, H.-K. Li, and H.-Y. Wang (2013a), Tectonic framework and evolution of the Tarim Block in NW China, *Gondwana Res.*, *23*, 1306–1315, doi:10.1016/j.gr.2012.05.009.

Zhang, Z., Y. Deng, L. Chen, J. Wu, J. Teng, and G. Panza (2013b), Seismic structure and rheology of the crust under mainland China, *Gondwana Res.*, *23*, 1455–1483, doi:10.1016/j.gr.2012.07.010.

Zhang Guo-Min, M. H.-S., W. Hui, and W. Xin-Lin (2005), Boundaries between active-tectonic blocks and strong earthquakes in China mainland, *Chin. J. Geophys.*, *48*, 662–671.

Zheng, Y.-F., W.-J. Xiao, and G. Zhao (2013), Introduction to tectonics of China, *Gondwana Res.*, *23*, 1189–1206, doi:10.1016/j.gr.2012.10.001.

Zhu, D.-C., Z.-D. Zhao, Y. Niu, Y. Dilek, Z.-Q. Hou, and X.-X. Mo (2013), The origin and pre-Cenozoic evolution of the Tibetan Plateau, *Gondwana Res.*, *23*, 1429–1454, doi:10.1016/j.gr.2012.02.002.

Ziegler, P. A., J.-D. van Wees, and S. Cloetingh (1998), Mechanical controls on collision-related compressional intraplate deformation, *Tectonophysics*, *300*, 103–129, doi:10.1016/S0040-1951(98)00236-4.

Zoback, M. L. (1992), First- and second-order patterns of stress in the lithosphere: The World Stress Map Project, *J. Geophys. Res.*, *97*, 11,703–11,728, doi:10.1029/92JB00132.